Rotor Fault Detection and Identification on a Hexacopter under Varying Flight States Based on Global Stochastic Models

Airin Dutta PhD Student
Michael McKay PhD Student
Fotis Kopsaftopoulos Assistant Professor
Farhan Gandhi Redfern Professor Director

Center for Mobility with Vertical Lift (MOVE)
Rensselaer Polytechnic Institute, Troy, NY

ABSTRACT

This work introduces the use of "global" stochastic models to detect and identify rotor failures in multicopters under different operating conditions, turbulence, and uncertainty. The identification of an extended class of time-series models known as Vector-dependent Functionally Pooled AutoRegressive models, which are characterized by parameters that depend on both forward velocity and gross weight, using scalar or vector aircraft response signals under white noise excitation has been described. A concise overview of the residual based statistical decision making schemes for fault detection and identification of rotor failures is provided. The scalar and vector statistical models, along with residual variance and residual uncorrelatedness methods were validated and their effectiveness was assessed by a proof-of-concept application to aircraft flight for healthy and faulty states under severe turbulence and intermediate operating conditions. The results of this study demonstrate the effectiveness of all the proposed residual-based time series methods in terms of prompt rotor fault detection, although the methods based on Vector AutoRegressive models exhibit improved performance compared to their scalar counterparts with respect to their performance in identifying rotor failures in the post-failure controller compensated state.

NOTATION

α	:	Type I risk level
β	:	Type II risk level
γ	:	Autocorrelation
τ	:	Lag
σ^2	:	Residual variance
$\boldsymbol{\Sigma}$	:	Residual covariance matrix
$E\{\cdot\}$	:	Expected value
PE	:	Prediction Error
PSD	:	Power Spectral Density
BIC	:	Bayesian Information Criterion
RSS	:	Residual Sum of Squares
ACF	:	Auto-Covariance Function
iid	:	identically independently distributed
SPP	:	Samples Per Parameter
LS	:	Least Squares
SSS	:	Signal Sum of Squares
AR	:	Scalar AutoRegressive model
VAR	:	Vector AutoRegressive model
FP	:	Functionally Pooled
VFP	:	Vector Functionally Pooled

Presented at the VFS International 76th Annual Forum & Technology Display, Virginia Beach, Virginia, USA, October 6–8, 2020.

INTRODUCTION

In recent years there has been immense interest in urban air mobility (UAM), enabled by autonomous electric VTOL (eVTOL) aircraft, as a revolutionary solution to extreme roadway congestion in major cities. A NASA sponsored study concluded UAM is a viable option and assessed its available market value at $500B (Ref. 1), but enabling widespread access to transportation services in dense urban environments requires real-time system-level awareness and safety assurance. As rotorcraft are complex systems with strong dynamic coupling between rotors, fuselage, and control inputs, they pose significant system modelling and identification challenges when compared to fixed-wing aircraft. These issues, as well as potential solutions, have been explored in the recent literature. Fault tolerant control for multi-rotors (Refs. 2, 3), as well as various fault diagnosis methods for helicopters have also been proposed (Refs. 4–6).

Statistical time series methods have been used to detect various fault types in aircraft systems due to their simplicity, efficient handling of uncertainties, no requirement of physics-based models, and applicability to different operating conditions (Refs. 7–10). Dimogianopoulos *et al.* (Ref. 11) have demonstrated the effectiveness of statistical schemes based on a Pooled Non-Linear AutoRegressive Moving Average with eXogenous excitation

(P-NARMAX) representation that models the pilot input and aircraft pitch rate to detect and isolate aircraft systems faults under different flight conditions, turbulence levels, and fault scenarios. In another study, reliable fault detection and identification have been achieved under unknown external disturbances and various maneuvering settings by modelling relationships among aircraft attitude data via stochastic Time-dependent Functionally Pooled Non-linear AutoRegressive with Exogenous excitation (TFP-NARX) representations (Ref. 12).

Kopsaftopoulos and Fassois formulated a novel stochastic identification framework based on the postulation of Vector-dependent Functionally Pooled ARX (VFP-ARX) models that employ data records obtained under varying operating conditions and uncertainty in order to identify a "global" model of the system dynamics (Refs. 13–15). The functional pooling concept is used to represent dynamics under multiple operating conditions and has been further expanded to model vector excitation-response signals in Refs. 16, 17. This identification framework incorporates parsimonious VFP models that can fully account for data cross-correlations among the operating conditions, perform functional pooling for the simultaneous treatment of all data records, and achieve statistically optimal parameter estimation based on Least Squares (LS) and Maximum Likelihood (ML) schemes. Moreover, novel approaches for online rotor fault detection and identification in multicopters using knowledge-based, statistical time series, and time-series assisted machine learning methods under different levels of turbulence and uncertainty have been recently studied in Refs. 18–20 .

The objective of the present study is the introduction and assessment of a novel online rotor fault detection and identification framework based on a stochastic "global" model of the healthy rotorcraft that accounts for varying operating conditions in the face of turbulence and uncertainty. More specifically, the cornerstone of the proposed framework lies on the identification of stochastic VFP models that can accurately represent the dynamics of a hexacopter under varying forward velocity and gross weight configurations. These models can subsequently enable online fault detection and identification via statistical decision making schemes based on residual properties under predetermined confidence levels (type I and II error probabilities, i.e., false alarm and missed faults).

HEXACOPTER MODEL AND DATA GENERATION

Physics-Based Modelling of Multicopter System

A flight simulation model has been developed for a regular hexacopter (Fig. 1) using summation of forces and moments to calculate aircraft accelerations. This model is used as the source of simulated data under varying operating and environmental conditions, as well as different fault types. Rotor loads are calculated using Blade Element Theory coupled with a 3×4 Peters-He finite state dynamic wake model (Ref. 21). This model allows for the simulation of abrupt rotor failure by ignoring the failed rotor inflow states and setting the output rotor forces and moments to zero.

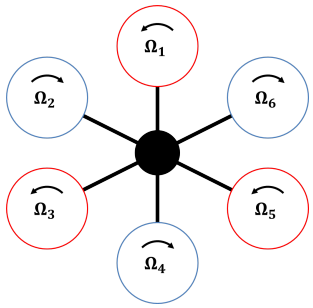

Figure 1: Schematic representation of a regular hexacopter

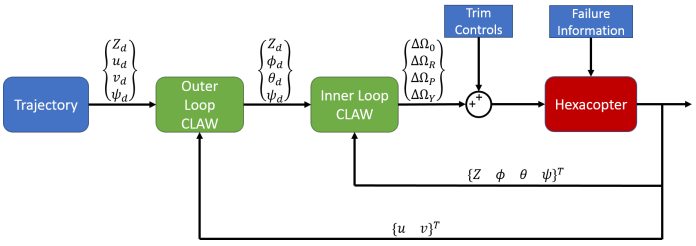

Figure 2: Controller Block Diagram

A feedback controller is implemented on the nonlinear model to stabilize the aircraft altitude and attitudes, as well as track desired trajectories written in terms of the aircraft velocities. This controller is designed at multiple trim points, with gain scheduling between these points to improve performance throughout the flight envelope.

The state vector consists of the 12 rigid body states and is defined in Eq. 1.

$$\mathbf{x} = \{X \quad Y \quad Z \quad \phi \quad \theta \quad \psi \quad u \quad v \quad w \quad p \quad q \quad r\}^T \tag{1}$$

The input vector is comprised of the first four independent multirotor controls for collective, roll, pitch and yaw and is defined in Eq. 2:

$$\mathbf{u} = \{\Omega_0 \quad \Omega_R \quad \Omega_P \quad \Omega_Y\}^T \tag{2}$$

The control architecture is illustrated in Fig. 2 and detailed in Ref. 2. This control design has been demonstrated to perform well even in the event of rotor 1, 2 or 6 failure, with no adaptation in the control laws themselves.

Data Generation

A continuous Dryden wind turbulence model (Ref. 22) has been implemented in the flight simulation model. The Dryden model is dependent on altitude, length scale, and turbulence intensity and outputs the linear and angular velocity components of continuous turbulence as spatially varying stochastic signals. The proper combination of these parameters determines the fit of the signals to observed turbulence. In this system, altitude is taken as 5 m (16.4 ft) and the length scale as the hub-to-hub distance of the hexacopter, which is 0.6096 m (2 ft). The data sets for aircraft states are generated through a series of simulations for different forward velocities and gross weights under severe level of turbulence for healthy aircraft. Similarly, data has also been generated for different rotor failures under different operating conditions. Note that the rotor failures addressed in this work are: front rotor (rotor 1), right-side rotor (rotor 2), and left-side rotor (rotor 6) failure (See Fig. 1).

Model identification is based on the stochastic aircraft output signals obtained under white noise excitation (Ref. 23) of the multirotor controls (Ref. 24) corresponding to a set of admissible flight states (operating conditions). The excitation ensures that the relevant rigid body modes have been properly excited so that the model estimated on basis of these signals describes the system adequately. A sample of K_1 values of forward velocity are used, represented by k^1 (first element of vector $\boldsymbol{k}$) and a sample of K_2 values are used for gross weight, represented by k^2 (second element of vector $\boldsymbol{k}$). A total of $K_1 \times K_2$ healthy flight simulations (one for each element of $\boldsymbol{k}$) are run, with the complete series covering the required range of each scalar parameter, say $[k^1_{min}, k^1_{max}] = [2, 12]$ m/s and $[k^2_{min}, k^2_{max}] = [2, 5]$ kg , via discretizations $k^1 = [k^1_1, k^1_2 \ldots, k^1_{K_1}] = [2,\ 3,\ 4,\ \ldots 10,\ 11,\ 12]$ m/s and $k^2 = [k^2_1, k^2_2, \ldots, k^2_{K_2}] = [2,\ 3,\ 4,\ 5]$ kg. For each flight state (defined by vector $\boldsymbol{k}$), data is recorded from simulations at a sampling frequency, $F_s = 1000$ Hz, to avoid any numerical instability issues. In the case of any rotor failure, the aircraft is unable to recover at lower and higher forward velocities for high gross weights. This is due to the fact that without changing the rotor size, the total thrust required to fly the aircraft in these conditions is not attainable within rotor speed limitations. Hence, the rotor failure models are based on datasets generated with similar white noise excitation but under restricted operating conditions as shown in Table 1.

Test data sets for validating the models and methods have been also generated without any excitation (because the system will not be actively excited during real flight) and under severe turbulence for some intermediate "unmodelled" (not used in baseline modelling) grid of operating conditions, like forward velocity of $[3.5, 4.5, \ldots, 11.5]$ m/s and gross weight of $[2.25, 2.5, 2.75, 3.25, 3.5, 3.75]$ kg.

Table 1: Training Data

Aircraft state	Velocity Range (m/s)	Gross Weight Range (kg)
Healthy Aircraft	$[2, 3, \ldots, 12]$	$[2, 3, 4, 5]$
Rotor 1, 2, 6 Failure	$[4, 5, \ldots, 9]$	$[2, 3, 4]$
Excitation: White Noise Signal length: 80 s For rotor failure signals, failure happens at 10 s Sampling frequency F_s: 1000 Hz Turbulence level: Severe		

General Workframe of Rotor Failure Detection and Identification

Let Z_o be signals that designate the aircraft under consideration in its healthy state, and Z_1, Z_2 and Z_6 the aircraft under fault of Rotor 1,2, and 6. Z_u designates the unknown (to be determined) state of the aircraft. Statistical learning methods explored in this study are based on discretized aircraft states signals $y[t]$[1] only (for $t = 1, 2, \ldots, N$). N denotes the number of samples and the conversion from discrete normalized time to analog time is based on $(t-1)T_s$, with T_s being the sampling period. The signals are represented by Z and subscript $(o, 1, 2, 6, u)$ is used to denote the corresponding state of the aircraft that produced the signals.

The signals generated from simulation are analyzed by non-parametric followed by parametric statistical methods and proper models are fitted and validated. Such models are trained for the cases Z_o, Z_1, Z_2, Z_6 in the baseline phase. Fault detection and identification (FDI) is performed in the online inspection phase by statistically comparing the information (residual based test statistics, Q) extracted from the current, unknown signals via the baseline models with predetermined baseline values. The general workframe of residual based FDI is depicted in Fig. 3.

BASELINE MODELLING OF THE AIRCRAFT

The aircraft signals for roll, pitch, and yaw attitudes generated via a series of simulations of forward flight and gross weight of the hexacopter under severe turbulence

[1] A functional argument in parentheses designates function of a real variable; for instance $x(t)$ is a function of analog time $t \in \mathbb{R}$. A functional argument in brackets designates function of an integer variable; for instance $x[t]$ is a function of normalized discrete time $(t = 1, 2, \ldots)$.

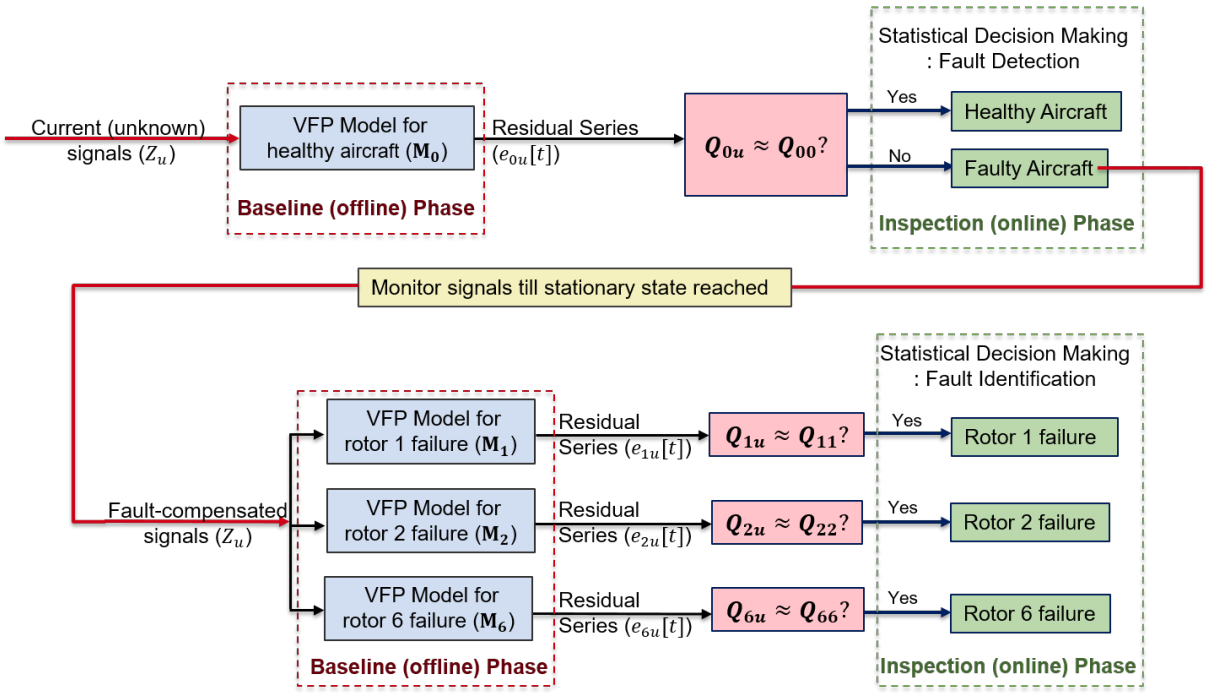

Figure 3: General workframe of global statistical time series methods for fault detection and identification.

for healthy and different faulty states are used for model identification. In the present scenario, response-only signals were obtained under white noise excitation $x[t]$.

Non-Parametric Identification

As a first step of the analysis, the non-parametric identification of the collected signals is based on the Welch-based power spectral density (PSD) estimate. The discrete Fourier transform of the signal of i-th window is given by:

$$Y_L^{(i)}[j\omega] = \frac{1}{\sqrt{L}} \sum_{t=0}^{L-1} y[t] \cdot w[t] \cdot e^{-j2\pi kt/N} \tag{3}$$

where L denotes the length of the window (w), and ω the frequency. Then, the Welch estimate of the PSD of a discrete-time signal is defined as follows:

$$\hat{S}_{yy}(\omega) = \frac{1}{K} \sum_{i=1}^{K} Y_L^{(i)}[j\omega] \cdot Y_L^{(i)}[-j\omega] \tag{4}$$

where K denotes the number of windows the signal is divided into. The PSD provides a description of the variation in the signal's power versus the frequency. It can provide a preliminary idea on the dynamic content of the signal.

Global Identification: Scalar VFP Model

The identification of a "global" Vector-dependent Functionally Pooled AutoRegressive (VFP-AR) model involves consideration of all admissible operating conditions. The data generated under the various forward velocities and gross weights (See Fig. 4) covering the required range of each variable is represented as follows:

$$\begin{aligned} &y_{\boldsymbol{k}}[t] \quad \text{with} \quad t = 1,2,...,N; \quad \boldsymbol{k} = \begin{bmatrix} k^1 & k^2 \end{bmatrix} \\ &k^1 \in \left[k_1^1, k_2^1, \ldots, k_{K_1}^1\right]; \quad k^2 \in \left[k_1^2, k_2^2, \ldots, k_{K_2}^2\right] \end{aligned} \tag{5}$$

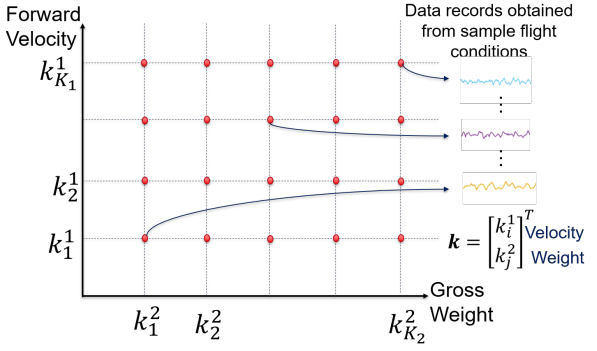

Figure 4: Schematic representation of data collection for the identification of a VFP model under different flight states characterized by varying forward velocity and gross weight.

with $y_{\mathbf{k}}[t]$ being the univariate response at some operating condition $\boldsymbol{k}_{i,j} = [k_i^1 \quad k_j^2]$.

The VFP-AR$(na)_{pa}$ model structure is of the following form:

$$\begin{aligned} y_{\boldsymbol{k}}[t] &= \sum_{i=1}^{na} a_i(\boldsymbol{k}) \cdot y_{\boldsymbol{k}}[t-i] + e_{\boldsymbol{k}}[t] \\ e_{\boldsymbol{k}}[t] &\sim \text{iid}\ \mathcal{N}(0, \sigma_e^2(\boldsymbol{k})), \qquad \boldsymbol{k} \in \mathbb{R}^2 \\ a_i(\boldsymbol{k}) &= \sum_{j=1}^{pa} a_{i,j} \cdot G_j(\boldsymbol{k}) \\ \mathbb{E}\{e_{\boldsymbol{k}_{i,j}}[t] \cdot e_{\boldsymbol{k}_{m,n}}[t-\tau]\} &= \gamma_e[\boldsymbol{k}_{i,j}, \boldsymbol{k}_{m,n}] \cdot \delta[\tau] \end{aligned} \tag{6}$$

where *na* designates the AutoRegressive (AR) order, $e_{\boldsymbol{k}[t]}$ the model's residual (one-step-ahead prediction error) sequence, that is a white (serially uncorrelated) zero mean sequence with variance $\sigma_e^2(\boldsymbol{k})$.This sequence should be serially uncorrelated but potentially cross-correlated with its counterparts corresponding to different simulations (different $\boldsymbol{k}$'s). The symbol $\mathbb{E}\{\cdot\}$ designates statistical expectation, $\delta[\tau]$ the Kronecker delta (equal to unity for $\tau = 0$ and equal to zero for $\tau \neq 0$) , $\mathcal{N}(\cdot,\cdot)$ Gaussian distribution with the indicated mean and variance, and iid stands for identically independently distributed. The AR parameters $a_i(\boldsymbol{k})$ are modeled as explicit functions of the vector $\boldsymbol{k}$ (which contains the forward velocity and gross weight components) by belonging to *pa*-dimensional functional subspace spanned by the mutually independent basis functions, referred to as the functional basis:

$$\mathscr{F}\langle a_i(\boldsymbol{k})\rangle = [G_1(\boldsymbol{k})\ G_2(\boldsymbol{k}) \ldots G_{pa}(\boldsymbol{k})] \tag{7}$$

The functional basis consists of polynomials of two variables (bivariate) obtained as cross products from their corresponding univariate polynomials (Chebyshev, Legendre, Jacobi, and other families of orthogonal polynomials, see Appendix A). In this work, Chebyshev type II polynomials are used as functional basis. The constants $a_{i,j}$ designate the AR coefficients of projection onto the functional basis. The identification of such parametric time series models is comprised of two main tasks: parameter estimation and model order selection.

The VFP-AR model is parameterized in terms of the parameter vector to be estimated[2] from the measured signals:

$$\widehat{\theta} \triangleq \begin{bmatrix} a_{1,1} & a_{1,2} & \ldots & a_{na,pa} \end{bmatrix} \tag{8}$$

[2]A hat designates estimator/estimate of the indicated quantity; for instance $\widehat{\boldsymbol{\sigma}}$ is an estimator/estimate of $\boldsymbol{\sigma}$.

and can be written in linear regression form as:

$$\begin{aligned} y_{\boldsymbol{k}}[t] &= \left[\varphi_{\boldsymbol{k}}^T[t] \otimes \mathbf{g}^T(\boldsymbol{k})\right] \cdot \theta + e_{\boldsymbol{k}}[t] \\ y_{\boldsymbol{k}}[t] &= \phi_{\boldsymbol{k}}^T[t] \cdot \theta + e_{\boldsymbol{k}}[t] \\ &\text{where:} \\ \varphi_{\boldsymbol{k}}[t] &\triangleq \left[y_{\boldsymbol{k}}[t-1] \ldots y_{\boldsymbol{k}}[t-na]\right]^T_{na\times 1} \\ \boldsymbol{g}(\boldsymbol{k}) &\triangleq \left[G_1(\boldsymbol{k}) \ldots G_{pa}(\boldsymbol{k})\right]^T_{pa\times 1} \\ \theta &\triangleq \left[a_{1,1} \ldots a_{na,pa}\right]^T_{(na\times pa)\times 1} \end{aligned} \tag{9}$$

Pooling together the expressions of the VFP-AR model corresponding to all vector operating parameters $\boldsymbol{k}$ $(\boldsymbol{k}_{1,1}, \boldsymbol{k}_{1,2}, \ldots, \boldsymbol{k}_{K_1,K_2})$ considered in the simulation yields:

$$\begin{aligned} &\begin{bmatrix} y_{\boldsymbol{k}_{1,1}}[t] \\ \vdots \\ y_{\boldsymbol{k}_{K_1,K_2}}[t] \end{bmatrix} = \begin{bmatrix} \phi_{\boldsymbol{k}_{1,1}}^T[t] \\ \vdots \\ \phi_{\boldsymbol{k}_{K_1,K_2}}^T[t] \end{bmatrix} \cdot \boldsymbol{\theta} + \begin{bmatrix} e_{\boldsymbol{k}_{1,1}}[t] \\ \vdots \\ e_{\boldsymbol{k}_{K_1,K_2}}[t] \end{bmatrix} \\ &\implies \boldsymbol{y}[t] = \boldsymbol{\Phi}[t] \cdot \boldsymbol{\theta} + \boldsymbol{e}[t] \end{aligned} \tag{10}$$

Substituting the data for $t = 1, 2, ..., N$ results in the following expression:

$$\begin{aligned} &\boldsymbol{y} = \boldsymbol{\Phi} \cdot \boldsymbol{\theta} + \boldsymbol{e} \\ &\text{where :} \\ &\boldsymbol{y} \triangleq \begin{bmatrix} \boldsymbol{y}[1] \\ \vdots \\ \boldsymbol{y}[N] \end{bmatrix}; \quad \boldsymbol{\Phi} \triangleq \begin{bmatrix} \boldsymbol{\Phi}[1] \\ \vdots \\ \boldsymbol{\Phi}[N] \end{bmatrix}; \quad \boldsymbol{e} \triangleq \begin{bmatrix} \boldsymbol{e}[1] \\ \vdots \\ \boldsymbol{e}[N] \end{bmatrix} \end{aligned} \tag{11}$$

Notice that despite its resemblance to standard regression, this expression includes a rich structure of interdependencies among the different variables and simulations, which need to be carefully taken into account. Furthermore, the term "functional pooling" signifies the functional dependence of each equation on the operating parameter vector $\boldsymbol{k}$. Using the above linear regression framework, the simplest approach for estimating the projection coefficient vector θ is based on minimization of the ordinary least squares (OLS) criterion $J^{OLS} := \frac{1}{N}\sum_{t=1}^{N} \boldsymbol{e}^T[t]\boldsymbol{e}[t]$. A better criterion according to the Gauss–Markov theorem (Ref. 25) is the weighted least squares (WLS) criterion:

$$J^{WLS} := \frac{1}{N}\sum_{t=1}^{N} \boldsymbol{e}^T[t]\boldsymbol{\Gamma}_{\boldsymbol{e}[t]}^{-1}\boldsymbol{e}[t] = \frac{1}{N}\boldsymbol{e}^T[t]\boldsymbol{\Gamma}_{\boldsymbol{e}^{-1}}\boldsymbol{e}_{[t]} \tag{12}$$

which leads to the weighted least squares(WLS) estimator:

$$\widehat{\theta}^{WLS} = \left[\boldsymbol{\Phi}^T\boldsymbol{\Gamma}_{\boldsymbol{e}}^{-1}\boldsymbol{\Phi}\right]^{-1}\left[\boldsymbol{\Phi}^T\boldsymbol{\Gamma}_{\boldsymbol{e}}^{-1}\boldsymbol{y}\right] \tag{13}$$

where $\boldsymbol{\Gamma}_{\boldsymbol{e}} = \mathbb{E}[\boldsymbol{e}\boldsymbol{e}^T]$ $(\boldsymbol{\Gamma}_{\boldsymbol{e}} = \boldsymbol{\Gamma}_{\boldsymbol{e}[t]} \otimes \boldsymbol{I}_N)$, where $\boldsymbol{I}_N$ is the $N \times N$ unity matrix) designates the residual covariance

matrix, which is practically unavailable. Nevertheless, it may be consistently estimated by applying (in an initial step) ordinary least squares (Ref. 26). Once $\widehat{\theta}^{WLS}$ is obtained, the final residual variance and residual covariance matrix estimates are calculated as:

$$\begin{aligned} \widehat{\sigma}_e^2(\boldsymbol{k},\widehat{\theta}^{WLS}) &= \frac{1}{N}\sum_{t=1}^{N} e_{\boldsymbol{k}}^2[t,\widehat{\theta}^{WLS}] \\ \widehat{\boldsymbol{\Gamma}}_{\boldsymbol{e}[t]} &= \frac{1}{N}\boldsymbol{e}[t,\widehat{\theta}^{WLS}]\boldsymbol{e}^T[t,\widehat{\theta}^{WLS}] \end{aligned} \tag{14}$$

The problem of VFP-AR model structure selection for a given basis function family consists of model order determination for the AR polynomials and determination of their corresponding functional subspaces. Usually, the AR model order is initially selected via customary model order selection techniques (Bayesian Information Criterion (BIC) and Residual Sum of Squares over Signal Sum of squares (RSS/SSS)) (Ref. 27) from individual datasets corresponding to a single cross-section (Ref. 18). A cross-section corresponds to a flight state defined by a pair of forward velocity and gross weight values, considered in the training dataset. Next, maximum functional subspace dimensionalities are considered, which define the search space of the functional subspace estimation subproblem. The exact subspace dimensionalities is decided by minimization of the BIC with respect to the candidate basis functions.

Model structure estimation may then be seen as the estimation of the integer-valued model structure vector $\boldsymbol{p}$, which to be uniquely defined, transformed into a binary variable vector as follows (Ref. 14):

$$\boldsymbol{p} \triangleq [(1,1),(1,2),\ldots,(K_1,K_2)]_{1\times(K_1K_2)} \tag{15}$$

Next, the selection of the final dimensionality may be based on minimization of the BIC (Ref. 14):

$$\begin{aligned} \widehat{\boldsymbol{p}} &= \arg\min_{\boldsymbol{p}} BIC(\boldsymbol{p}) \\ BIC(\boldsymbol{p}) &= \ln\mathbf{L} + dim(\theta)\cdot\ln\frac{NK_1K_2}{N} \\ \text{where,}\quad \mathbf{L} &= \sum \sigma_e^2(\boldsymbol{k}) \quad \forall \quad \boldsymbol{k}_{i,j} \\ & \qquad i=1,\ldots,K_1 \quad j=1,\ldots,K_2 \end{aligned} \tag{16}$$

The Residual sum of Squares over Signal Sum of Squares (RSS/SSS) for all the cross-sections used in model estimation is given by:

$$\begin{aligned} \frac{RSS}{SSS} &= \sum \frac{\sum_{t=1}^{N} e_{\boldsymbol{k}}^2[t]}{\sum_{t=1}^{N} y_{\boldsymbol{k}}^2[t]} \quad \forall \quad \boldsymbol{k}_{i,j} \\ & i=1,\ldots,K_1, \quad j=1,\ldots,K_2 \end{aligned} \tag{17}$$

Global Identification: Vector VFP Model

The identification of a Vector-dependent Functionally Pooled Vector AutoRegressive (VFP-VAR) model employs multivariate[3] (s-variate) time series modelling (Refs. 28, 29). Though their resemblance to their univariate (or scalar) counterparts, they have a richer structure as they can simultaneously model vector signals, that is signals collected from multiple outputs and/or inputs. The aircraft response (attitude) signals recorded under various operating conditions can be collectively represented as follows:

$$\begin{aligned} &\boldsymbol{y}_{\boldsymbol{k}}[t] \quad \text{with} \quad t=1,2,\ldots,N; \quad \boldsymbol{k}=\begin{bmatrix}k^1 & k^2\end{bmatrix} \\ &k^1 \in \begin{bmatrix}k_1^1,k_2^1\ldots,k_{K_1}^1\end{bmatrix}; \quad k^2 \in \begin{bmatrix}k_1^2,k_2^2\ldots,k_{M_2}^2\end{bmatrix} \end{aligned} \tag{18}$$

where $\boldsymbol{y}_{\boldsymbol{k}}[t]$ is the $(s\times 1)$ response vector at some operating condition $\boldsymbol{k}=[k_i^1 \quad k_j^2]$.

The VFP-VAR$(na)_{pa}$ model structure is of the following form:

$$\begin{aligned} \boldsymbol{y}_{\boldsymbol{k}}[t] &= \sum_{i=1}^{na}\mathbf{A}_i(\boldsymbol{k})\boldsymbol{y}_{\boldsymbol{k}}[t-i]+\boldsymbol{e}_{\boldsymbol{k}}[t] \\ \boldsymbol{e}_{\boldsymbol{k}}[t] &\sim \text{iid}\,\mathcal{N}(0,\Sigma_{\boldsymbol{e}}(\boldsymbol{k})), \qquad \boldsymbol{k}\in\mathbb{R}^2 \\ \mathbf{A}_i(\boldsymbol{k}) &= \sum_{j=1}^{pa}\mathbf{A}_{i,j}\cdot G_j(\boldsymbol{k}) \\ \mathbb{E}\{\boldsymbol{e}_{\boldsymbol{k}_{i,j}}[t]\cdot\boldsymbol{e}_{\boldsymbol{k}_{m,n}}^T[t-\tau]\} &= \Sigma_e[\boldsymbol{k}_{i,j},\boldsymbol{k}_{m,n}]\cdot\delta[\tau] \end{aligned} \tag{19}$$

with na designating the AutoRegressive (AR) model order, $\boldsymbol{e}_{\boldsymbol{k}}[t]$ is a $(s\times 1)$ innovations vector which is zero mean, serially uncorrelated, with fully parametrized cross–covariance matrices $\Sigma_{\boldsymbol{e}}(\boldsymbol{k})$. $\mathbb{E}\{\cdot\}$ designates statistical expectation, and $\delta(\tau)$ the Kronecker delta function. The AR matrices $\mathbf{A}_i(\boldsymbol{k})$ are fully parametrized and have dimension of $(s\times s)$. They are expressed as explicit functions of the operating parameter $\boldsymbol{k}$ by belonging to a functional subspace of dimensionality pa, spanned by the mutually orthogonal functions given by Eq. 7 which consists of polynomials bivariate variables (see Appendix A). These functions form a functional basis, and along with constant matrices $\mathbf{A}_{i,j}$ constitute the corresponding, fully parametrized, projection matrices $\mathbf{A}_i(\boldsymbol{k})$.

The VFP-VAR model is parametrized in terms of the parameter vector to be estimated in the following manner:

$$\widehat{\theta} \triangleq vec\Big(\begin{bmatrix}\mathbf{A}_{1,1} & \mathbf{A}_{1,2}\ldots\mathbf{A}_{na,pa}\end{bmatrix}^T\Big) \tag{20}$$

where $vec(\cdot)$ designates the operator that transforms the indicated matrix into a vector by stacking its columns.

[3] Bold–face upper/lower case symbols designate matrix/column–vector quantities, respectively. Matrix transposition is indicated by the superscript ^{T}.

The VFP-VAR model formulation in linear regression form can be written as:

$$\boldsymbol{y_k}[t] = \left[I_s \otimes \boldsymbol{\varphi_k}^T[t] \otimes \boldsymbol{g}^T(\boldsymbol{k})\right] \cdot \theta + \boldsymbol{e_k}[t]$$
$$\boldsymbol{y_k}[t] = \boldsymbol{\phi_k}^T[t] \cdot \theta + \boldsymbol{e_k}[t]$$

where:

$\boldsymbol{I_s}$ is the identity matrix of dimension $s \times s$

$$\boldsymbol{\varphi_k}[t] \triangleq \left[\boldsymbol{y_k}^T[t-1] \ldots \boldsymbol{y_k}^T[t-na]\right]^T_{(na\times s)\times 1}$$
$$\boldsymbol{g}(\boldsymbol{k}) \triangleq \left[G_1(\boldsymbol{k}) \ldots G_{pa}(\boldsymbol{k})\right]^T_{pa\times 1}$$
$$\theta \triangleq vec\left(\begin{bmatrix}\mathbf{A}_{1,1} & \mathbf{A}_{1,2} \ldots \mathbf{A}_{na,pa}\end{bmatrix}^T\right)_{(na\times s\times pa)\times 1} \quad (21)$$

Pooling together the expressions of the VFP-VAR model corresponding to all vector operating parameters $\boldsymbol{k}$ $(\boldsymbol{k}_{1,1}, \boldsymbol{k}_{1,2}, \ldots, \boldsymbol{k}_{K_1,K_2})$ considered in the simulation yields similar form as Eq. 10. Next, substituting the data for $t = 1,2,\ldots,N$ as before results in the expression similar to Eq. 11.

Estimation of the model parameters using the above linear regression framework follows in the similar way as scalar models given by Eq. 13. Model structure selection is also performed in the same two-step approach: (i) Determination of VAR order with data sets of single cross-sections based on the model selection criteria (Ref. 18) and (ii) functional basis dimensionality selections based on BIC minimization for the selected VAR order. Note that for vector models the term, $\sigma^2_{\boldsymbol{\hat{e}}}(\boldsymbol{k})$ in Eq. 16 is replaced by the trace of $\Sigma(\boldsymbol{k})$, the residual covariance matrix for a single cross-section. And, to determine the fit of the estimated models by RSS/SSS criteria given by Eq. 17, the Frobenius norm of the vector of residual, $\boldsymbol{e_k}[t]$ and signal, $\boldsymbol{y_k}[t]$ have been used.

RESIDUAL-BASED FAULT DETECTION AND IDENTIFICATION

For tackling fault detection and identification, model residual based methods use functions of the residual sequences (known as characteristic quantity, Q) which are obtained by driving the current signal(s) (Z_u) through the models estimated in the baseline phase for the healthy aircraft (M_o) and different fault types (M_1, M_2, M_6). The key idea is that the residual sequence obtained by a model that truly reflects the current state of aircraft possesses certain distinct properties which are distinguishable from that obtained from the other models. Note that the functional parameters or flight conditions are substituted in the functional part of VFP models to obtain the corresponding AR/VAR models for that particular flight condition, before filtering the current signals through them.

Let M_V designate the model representing the structure in its V state ($V = 0,1,2,6$), where "0" denotes healthy state and "1,2,6" signify the rotor which has failed in the faulty state. The residual series obtained by driving the current signal(s) (Z_u) through each one of the aforementioned models are designated as $\boldsymbol{e}_{0u}[t], \boldsymbol{e}_{1u}[t], \boldsymbol{e}_{2u}[t], \boldsymbol{e}_{6u}[t]$ and are characterized by variances $\sigma^2_{0u}, \sigma^2_{1u}, \sigma^2_{2u}, \sigma^2_{6u}$ respectively. The characteristic quantity can be the variance or the whiteness of the residual sequence as discussed in the following sections. The first subscript designates the model employed, while the second the aircraft state corresponding to the currently used response signal(s). The characteristic quantities obtained from the corresponding residual series are designated as $Q_{0u}, Q_{1u}, Q_{2u}, Q_{6u}$. The characteristic quantities obtained using the baseline data records are designated as $Q_{VV}(V = 0,1,2,6)$.

Residual Variance Method

In this method, the characteristic quantity used for fault detection is the residual variance (Ref. 7). Fault detection is based on the fact that the residual series $e_{ou}[t]$, obtained by driving the current signals, Z_u through the model, M_o (corresponding to the healthy state) should be characterized by variance $\sigma^2_{ou} = \sigma^2_{oo}$ which becomes minimal if and only if the current state of the aircraft is healthy ($Z_u = Z_o$). Fault detection is based on the following hypothesis testing procedure:

$$\begin{aligned} H_0 &: \sigma^2_{ou} \le \sigma^2_{oo} \quad \text{(null hypothesis – healthy aircraft)} \\ H_1 &: \sigma^2_{ou} > \sigma^2_{oo} \quad \text{(alternate hypothesis – rotor failure)} \end{aligned} \quad (22)$$

Under the null (H_o) hypothesis, the residuals $e_{ou}[t]$ are (just like the residuals $e_{oo}[t]$), iid Gaussian with zero mean and variance σ^2_{oo}. Hence the quantities $N_u \cdot \widehat{\sigma}^2_{ou}/\sigma^2_{oo}$ and $(N_o - d) \cdot \widehat{\sigma}^2_{oo}/\sigma^2_{oo}$ follow central χ^2 distribution with N_u and $N_o - d$ degrees of freedom, respectively (as sums of squares of independent standardized Gaussian random variables)[4]. N_o and N_u designate the number of samples used in estimating the residual variance in the healthy and current cases, respectively (typically $N_o = N_u = N$), and d designates the dimensionality of the estimated model parameter vector. N_u and N_o should be adjusted to $N_u - 1$ and $N_o - 1$, respectively, if each estimated mean is subtracted from each residual sequence. Consequently, the following statistic follows a Fischer distribution (denoted by F) with $(N_u, N_o - d)$ degrees of freedom as the ratio of two independent and normalized χ^2 random vari-

[4] A hat designates estimator/estimate of the indicated quantity; for instance $\widehat{\sigma}$ is an estimator/estimate of σ.

ables (Ref. 7):

$$\text{Under } H_0 : F = \frac{\dfrac{N_u\ \widehat{\sigma}_{ou}^2}{N_u\ \sigma_{oo}^2}}{\dfrac{(N_o-d)\ \widehat{\sigma}_{oo}^2}{(N_o-d)\ \sigma_{oo}^2}} = \frac{\widehat{\sigma}_{ou}^2}{\widehat{\sigma}_{oo}^2} \tag{23}$$

The following hypothesis test is thus constructed at the α type I (false alarm) risk level:

$$\begin{array}{ll} F \le f_{1-\alpha}(N_u, N_o-d) & \Longrightarrow H_0 \text{ accepted (healthy aircraft)} \\ \text{Else} & \Longrightarrow H_1 \text{ accepted (rotor failure)} \end{array} \tag{24}$$

where, $f_{1-\alpha}(N_u, N_o-d)$ designates the corresponding Fischer distribution's $(1-\alpha)$ critical point.

Fault identification may be similarly achieved via pairwise tests of the form:

$$\begin{array}{lll} H_0 & : & \sigma_{Xu}^2 \le \sigma_{XX}^2 \quad \text{(aircraft under Rotor X failure)} \\ H_1 & : & \sigma_{ou}^2 > \sigma_{oo}^2 \quad \text{(aircraft not under Rotor X failure)} \end{array} \tag{25}$$

Note that the baseline residual variance, $\sigma_{VV}^2(\boldsymbol{k})$ $(V = 0,1,2,6)$ are available only for the modelled cross-sections, $\boldsymbol{k}_{i,j}\forall$. However, during online monitoring "unmodelled", intermediate operating conditions may be encountered. The model representing the dynamics at that particular condition will be obtained by substituting the values of forward velocity and gross weight into the functional basis. But, if there is no baseline data set available for this particular operating values, the baseline residual sequence, required for statistical comparison with the current residual sequence, cannot be obtained. The aforementioned problem can be tackled via the the projection of the known variance values onto bivariate polynomial subspaces, similar to Eq. 7, in order to calculate the residual variance for any intermediate operating condition without having a corresponding baseline data set, thus facilitating FDI within the entire operating range.

Residual Uncorrelatedness Method

This method is based on the fact that the residual series $\boldsymbol{e}_{ou}[t]$, obtained by driving the current signals (Z_u) through the model (M_0), is uncorrelated (white) if and only if the aircraft is currently in its healthy condition (Ref. 7). Fault detection is performed by the following hypothesis testing:

$$\begin{array}{lll} H_0 & : & \rho[\tau] = 0 \quad \text{(null hypothesis – healthy aircraft)} \\ H_1 & : & \rho[\tau] \ne 0 \quad \text{(alternate hypothesis – rotor failure)} \end{array} \tag{26}$$

where $\rho[\tau]$ is the normalized autocorrelation function $(\rho_{xx}[\tau] = \gamma_{xx}[\tau]/\gamma_{xx}[0])$ of the residual sequence $\boldsymbol{e}_{ou}[t]$.

Therefore, the characteristic quantity for fault detection by this method is $\left[\rho[1]\ \rho[2]\ \rho[3]\ldots\ \rho[\tau]\right]^T$. For this method, r is the design variable for the statistical test, which denotes the maximum lag in time (τ) for which the normalized ACFs are being accounted for. Under the null hypothesis (H_0), the residuals $\boldsymbol{e}_{ou}[t]$ are iid Gaussian with zero mean and the test statistic χ_ρ^2 follows a χ^2 distribution with r degrees of freedom, given as:

$$\text{Under } H_0 : \chi_\rho^2 = N(N+2)\cdot\sum_{\tau=1}^{r}(N-\tau)^{-1}\cdot\widehat{\rho}[\tau]^2 \sim \chi^2(r) \tag{27}$$

where $\widehat{\rho}[\tau]$ denotes the estimator of $\rho[\tau]$.

Statistical decision making is achieved by the following test for α (false alarm) risk level:

$$\begin{array}{ll} \chi_\rho^2 \le \chi_{1-\alpha}^2(r) & \Longrightarrow H_0 \text{ is accepted (healthy aircraft)} \\ \text{Else} & \Longrightarrow H_1 \text{ is accepted (rotor failure)} \end{array} \tag{28}$$

where $\chi_{1-\alpha}^2(r)$ denotes the χ^2 distribution's $1-\alpha$ critical point.

Fault identification is achieved by similarly examining which one of the $\boldsymbol{e}_{Vu}[t]$ $(V = 1,2,6)$ residual series is statistically uncorrelated.

RESULTS AND DISCUSSION

Data Generation

Flight simulation for the hexacopter was performed at operating ranges specified in Table 1 with white noise excitation under severe turbulence according to the Dryden model. Figures 5 and 6 show pitch time histories for the hexacopter, for cases of healthy flight and rotor 1 failure. For the simulation results presented, rotor failure occurs at $t = 10$ s, indicated by the vertical dashed line. It should be noted that due to failure, the signals show a sharp transient response before settling down to a controller-compensated steady state. The failure detection takes place in the transient part of the signal, whereas the failure identification takes places in the fault compensated steady state, since the models are suitable for modelling stationary signals only.

Some observations on how the roll, pitch and yaw signals deviate due to failure determined by the dynamic knowledge of the hexacopter is discussed in Ref. 18. This paper demonstrates the indicative results for severe level of turbulence only, while results from moderate and low levels of turbulence will be presented in a subsequent publication.

Non-Parametric Analysis of signals

The roll and pitch signals of the healthy aircraft obtained for some particular cross-section (a point in the grid of forward velocity and gross weight) were analysed

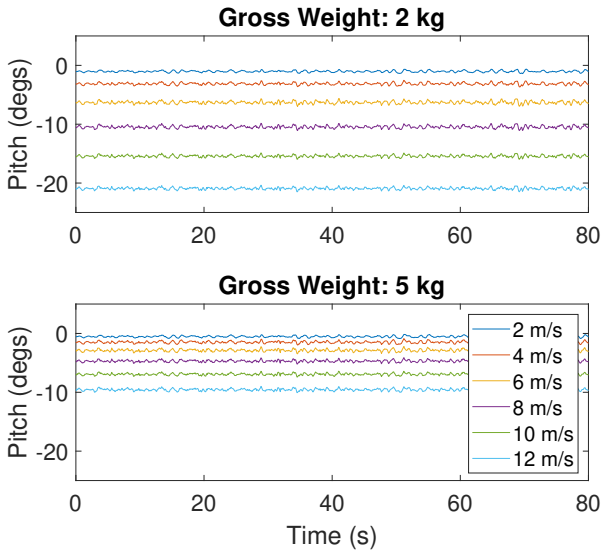

Figure 5: Pitch Time History, Healthy Aircraft

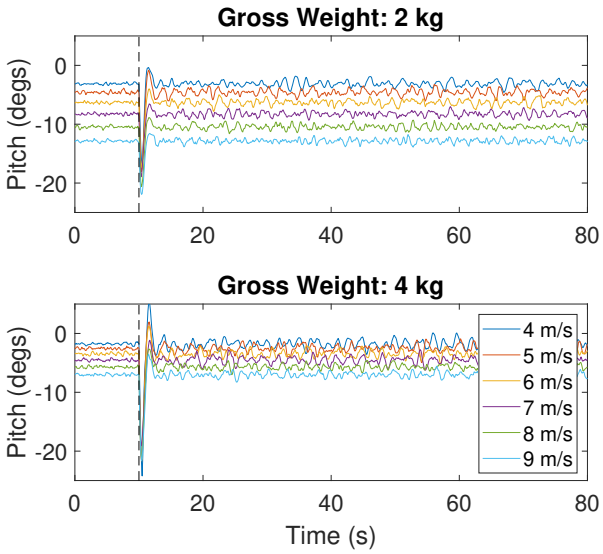

Figure 6: Pitch Time History, Rotor 1 failure

(since the important dynamics of a hexacopter lies in the lateral and longitudinal modes) by Welch method with $N = 80,000$ samples ($F_s = 1000$ Hz, window size of 800, nfft of 2000, overlap of 90%; Matlab function *pwelch.m*). The system dynamics are observed to lie in the range of $0.02 - 2$ Hz. Hence, the signals were downsampled to a sampling frequency of $F_s = 10$ Hz such that the frequency range of interest is $0 - 5$ Hz.

Next, the Welch-based non-parametric analysis for the downsampled signals for a few indicative cross-sections were repeated to observe whether there is any effect of the operating conditions on system dynamics. The parameters used were as follows: $N = 800$ samples, window size of 200, nfft equal to the window size, and overlap of 95%. This was performed to justify the need for complex models that can represent the change in dynamics of the hexacopter due to different forward velocity and gross weight. Table 2 shows the there is change in the 1st mode for both lateral and longitudinal modes of the healthy aircraft with change in forward velocity, but not with gross weight.

Table 2: Effect of operating conditions on system modes

Gross Weight (kg)	Forward Velocity (m/s)		
	2	7	12
2	0.6/0.5	0.8/ 0.4	0.85/0.8
3	0.6/0.5	0.8/0.4	0.85/0.8
5	0.6/0.5	0.8/0.4	0.85/0.8

All the frequencies are given in Hz
1st longitudinal/lateral mode (pitch/ roll signals)

Scalar VFP-AR model based Fault Detection and Identification

Model Identification Conventional AR models representing the healthy aircraft are obtained through standard identification procedures (Refs. 18, 20) based on obtained pitch signals (80 s, $N = 800$ samples long, Matlab function *ar.m*) for some cross-sections. This leads to an AR(15) model, which is used as a reference and for providing approximate orders for the corresponding "global" models representing the aircraft dynamics for the entire range.

The vector functionally pooled model for the healthy aircraft is based on signals of the same length obtained from a total of $K_1 \times K_2 = 11 \times 4 = 44$ simulations, for 11 values of forward speed and 9 values of gross weight covering the entire admissible operating range. Functional basis order selection starts with the maximum functional search space consisting of 1035 Chebyshev Type II bivariate polynomial basis functions (see Appendix A). The final functional basis order selected was 3 and 1 ($\mathbf{p} = 9$) for speed and weight variables, respectively, based on the minimum BIC criterion (Eq. 16), as depicted in Fig. 7. This implies that the dynamics of the healthy aircraft as represented by this model vary in a quadratic fashion with the forward velocity, but is constant with respect to the gross weight. This model was validated by checking the whiteness (uncorrelatedness) and the normality of the model residuals (Matlab functions *acf.m* and *normplot.m*, respectively) for all the cross-sections (See Appendix B).

Indicative PSD magnitude curves, depicted in Figs. 15a and 15b (See Appendix C), illustrates that the frequency spectrum obtained from the healthy aircraft model varies

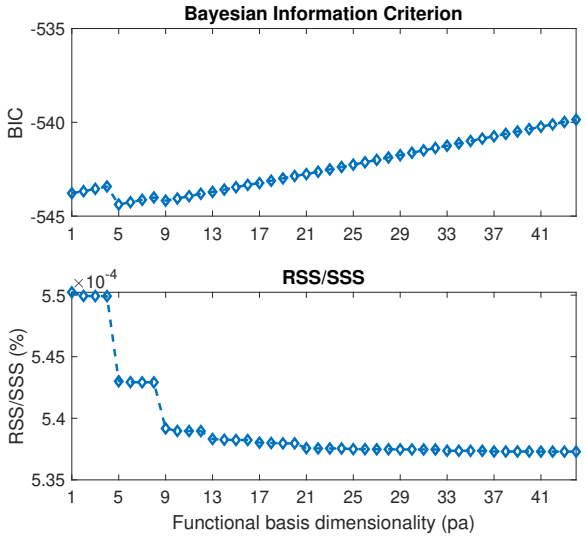

Figure 7: VFP-AR Model Structure Selection

with velocity but is constant with the gross weight. This observation is consistent with the preliminary non-parametric analysis which also shows no change in dynamics with varying gross weight.

The VFP-AR models for different rotor failures estimated with the pitch signal obtained from the post failure fault-compensated stationary state are identified in a similar way. But the number of datasets available are $K_1 \times K_2 = 6 \times 3 = 18$, and therefore functional search space is limited by the admissible range of operation under rotor failure. The summary of the VFP models estimated for healthy and faulty states are given in Table 3.

Fault Detection and Identification In this section, indicative FDI results based on scalar versions of the vector functionally pooled time series models utilizing the pitch signal have been presented. The current pitch signals are generated at some random but known forward velocity and gross weight (within the admissible operating range) under ambient excitation due to severe turbulence only. The model parameters for the healthy AR model are calculated by substituting the known values of $\mathbf{k} = [k^1 \quad k^2]$ in the functional basis of the VFP-AR model for healthy aircraft. Next, the current signals were driven through this identified healthy AR model for that particular operating condition to generate residual sequences. Fault detection was attempted through characteristic quantities which are functions of the residual sequences, as previously discussed.

Table 3: Model identification summary results.

Aircraft State	Model Selected	No. of parameters
Healthy Aircraft	VFP-AR$(15)_9$	135
	VFP-VAR$(2)_9$	162
Rotor 1 Failure	VFP-AR$(11)_4$	44
	VFP-VAR$(3)_4$	108
Rotor 2 Failure	VFP-AR$(8)_4$	32
	VFP-VAR$(3)_7$	189
Rotor 6 Failure	VFP-AR$(7)_4$	28
	VFP-VAR$(3)_7$	189

Scalar models are estimated with pitch signals only
Vector models are estimated with roll, pitch & yaw signals
Model order is denoted in brackets
Functional order is denoted in subscript

Similarly, in the event of a rotor fault, the steady state residuals are generated from each of the VFP-AR models for rotor failure, parametrized as AR models for the current operating condition. Fault identification was achieved using their properties for decision making through multiple binary hypothesis tests. In the current study, the fault cases considered are related to failure of rotor 1, 2 and 6. Therefore, there are 3 fault hypotheses and the corresponding hypothesis tests have to be carried out simultaneously.

Residual Variance Method Fault detection is achieved in an online, real-time manner through taking a 5 s ($N = 50$ samples) moving window of the current signal with the window being updated every 0.1 s. Then, the windowed data is filtered through the healthy model estimated for the current operating condition to generate the residual sequence of the same length. The variance of the generated residuals is statistically compared to the corresponding baseline residual variance. The baseline residual variance for the current operating condition is estimated from a bivariate polynomials (Eq. 7) model fitted to the residual variances of the modelled operating conditions, with the model structure being selected by RSS/SSS criteria. The critical limit is determined from the F distribution's $(1-\alpha)$ critical limit for $(50, 35)$ degrees of freedom. The hypothesis test is conducted at the α (false alarm) risk level of 10^{-3} and indicative results for different states of the aircraft (healthy, front, and side rotor failure) flying at 3.5 m/s and having a gross weight of 3.75 kg are presented in Fig. 8a. In both the figures, the vertical black and the horizontal red dashed lines represent the time of rotor failure and the critical limit (threshold), respectively. A fault is detected when the F statistic exceeds the critical limit at the designated type I risk level.

Since a minimum number of 50 samples are required so that the test is statistically significant with minimum false alarms, the test starts at 5 s. For the current pitch signals coming from a healthy flight, the test statistics (Eq. 22) always remain below the critical limit for the test, hence the null hypothesis (that it is a healthy case) is accepted. In the case of signals generated from an aircraft with rotor

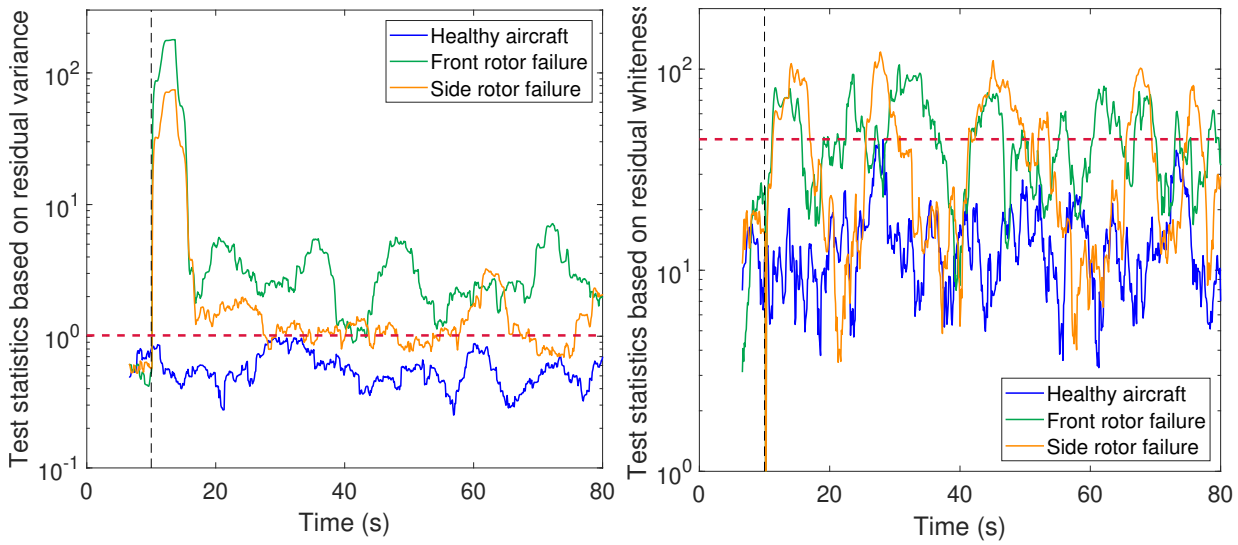

(a) Residual variance

(b) Residual uncorrelatedness

Figure 8: Indicative fault detection results based on the pitch residual signals obtained via VFP-AR model of healthy aircraft. The dashed vertical line represents the time of rotor failure. The dashed red horizontal line indicates the statistical threshold at the respective α risk levels. A fault is detected when the statistic exceeds the threshold.
(a) Residual variance method; operating condition: 3.5 m/s, 3.75 kg and $\alpha = 10^{-2}$ (b) Residual uncorrelatedness method; operating condition: 4.5 m/s, 2.5 kg and $\alpha = 10^{-6}$.

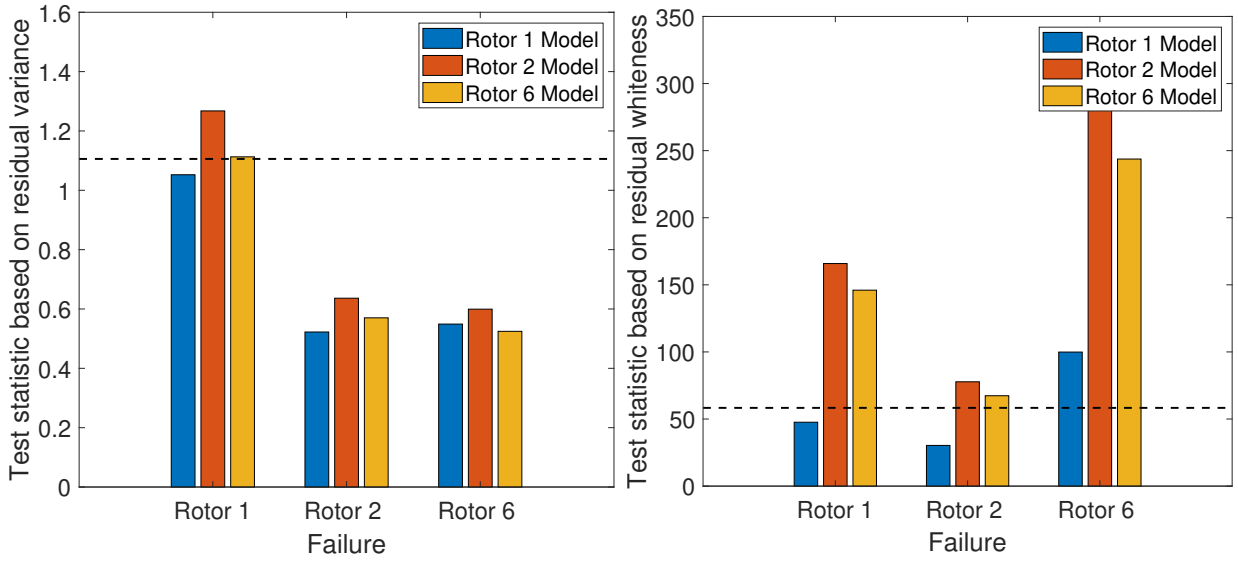

(a) Residual variance

(b) Residual uncorrelatedness

Figure 9: Indicative fault identification results based on the pitch residual signals obtained via VFP-AR model of different rotor failures. The dashed black horizontal line indicates the statistical threshold at the respective α risk levels. (a) Residual variance method; operating condition: 7.5 m/s, 2.5 kg and $\alpha = 0.25$ (b) Residual uncorrelatedness method; operating condition: 8.5 m/s, 3.5 kg and $\alpha = 10^{-3}$.

failure, the fault detection at the time of failure is immediate (within 0.1 s, which is the window update interval), showing a violation of the critical limit. Thus, the alternate hypothesis of faulty aircraft is accepted.

Post online fault detection, the variance of the signals is monitored until steady state is reached (Ref. 20). For fault identification, the current signals, under the fault-compensated state of the aircraft, of length 20 s ($N = 200$

samples) updated every 1 s, are filtered through the corresponding baseline scalar models for rotor 1, 2, and 6 failure, parametrized for the current operating condition. The residual variances denoted as σ^2_{1u}, σ^2_{2u} and σ^2_{6u}, respectively, are statistically compared with their nominal values, namely σ^2_{11}, σ^2_{22} and σ^2_{66}. Note that each of these baseline values are estimated via bivariate polynomial models fitted to the residual variances for modelled operating conditions in the baseline phase. Indicative fault identification results for a single time window of pitch signals obtained under severe turbulence at 7.5 m/s and 2.5 kg are presented in Fig. 9a. When the test statistic of the residual obtained from M_1 lies below the critical limit constructed at the α (false alarm) risk level of 0.25, and exceeds it for the residuals obtained from the other two models (M_2 and M_6), the fault is correctly identified as rotor 1 failure. Fault identification follows for the other types of failure in similar way. However, if the test statistics obtained from two or more models lie below the critical limit, then confusion in identifying the faulty rotor is implied. If all the test statistics exceed the critical limit, no decision is made. For side rotor (2 and 6) failure signals, in Fig. 9a the test statistics obtained from all three rotor failure models lie below the critical limit. This implies multiple decision, and hence misclassification error between the three rotors.

Residual Uncorrelatedness Method Online fault detection via the residual uncorrelatedness method is performed in a similar manner, with the same window length and update interval, as discussed in the residual variance method. In this method, the test statistics (Eq. 26) based on the autocorrelation function of the residuals generated from the current pitch signals. After a preliminary investigation of the effect of the maximum lag τ on the method's performance, a value of 30 has been chosen as adequate. Hence, the $(1-\alpha)$ critical point of a χ^2 distribution with 30 degrees of freedom denotes the critical limit for the statistical hypothesis testing. Figure 8b shows indicative results for different aircraft states for healthy, front and side rotor failure cases, respectively, at the 10^{-1} risk level α. The test signals are obtained under severe turbulence, forward velocity of 4.5 m/s, and gross weight 2.5 kg. The test statistics crossing over the critical limit (dashed red line) denote rejection of the null hypothesis, thus declaring fault detection. Due to the fault-induced sharp transients in the signals, the fault detection is immediate.

After the fault is compensated for by the controller, pitch signals of length 20 s ($N = 200$ samples), updated every 1 s are filtered through faulty models M_1, M_2 and M_6 to generate residuals $e_{1u}[t]$, $e_{2u}[t]$ and $e_{6u}[t]$, respectively. The autocorrelation function of the residual sequences with maximum lag $\tau = 30$ has been considered as the test statistic in order to classify faults. The critical limit of a χ^2 distribution with 30 degrees of freedom for the statistical hypothesis testing has been constructed at the α (false alarm) risk level of 10^{-3}.

The results obtained from a single window of 20 s for different rotor failures signals at operating conditions, 8.5 m/s and 3.5 kg are shown in Fig. 9b. It can be observed that when a pitch signal from rotor 1 failure is filtered through M_1, the residuals are uncorrelated, and they are correlated if obtained from models M_2 and M_6, as evident for the test statistic being below the critical limit in the former and exceeding it in the latter two cases. This method also faces significant challenges in tackling fault identification as evident from Fig. 8b, where in the cases of rotor 2 and 6 failures, the decisions made are front rotor failure and no decision, respectively.

Vector VFP-VAR model based Fault Detection and Identification

Model Identification Vector functionally pooled - vector (multivariate) AutoRegressive identification of the healthy aircraft has been based on 80 s ($N = 800$ samples at sampling frequency 10 Hz) data sets for the roll, pitch, and yaw signals, with white noise excitation and ambient excitation due to turbulence (assumed to be white) generated from 44 flight simulations covering the entire operating range. Model VFP-VAR$(2)_9$ has been selected to represent healthy dynamics over the entire operating range by following the same procedure as the scalar counterpart:(1) Vector AutoRegressive order has been chosen by BIC (Ref. 18) as VAR(2) based on datasets from a few cross-sections (2) Functional basis order selected from the same maximum functional search via minimum BIC (Eq. 16). According to Fig. 10 the functional basis dimesionality is chosen as (3,1) (each functional subspace consists of $\mathbf{p} = 9$ Chebyshev Type II two-dimensional polynomials), depicting quadratic and constant relation with respect to velocity and weight respectively. The chosen model is validated by examining whether the model residuals are normal and uncorrelated for all cross-sections (See Appendix B).

The vector counterpart of VFP models for rotor failures are identified in a similar fashion but for the limited operating range and the details are given in Table 3.

Fault Detection and Identification In this section, few indicative FDI results based on vector (multivariate) versions of the vector functionally pooled time series models are presented. The test signals (ordered roll, pitch, yaw) are acquired for flight simulation under severe turbulence for which the operating conditions are known. The model parameters for the healthy VAR model are calculated by substituting the known values of forward

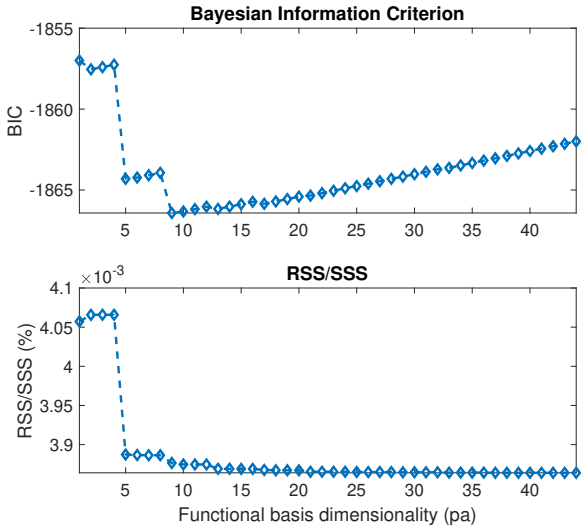

Figure 10: VFP-VAR Model Structure Selection

velocity and gross weights in the functional basis of the VFP-VAR model for the healthy aircraft. Next, the current signals driven through this identified healthy VAR model for that particular operating condition yield three sets of residual sequences. The residual based fault detection is performed by the statistical comparison of each characteristic quantity obtained via the current residual sequence with the corresponding baseline quantity. In other words, the characteristic quantity obtained from the current roll residual sequence is compared to the baseline quantity obtained from the roll residual sequence and so on. Therefore, the statistical hypothesis testing is performed thrice for a particular time window (duration of signal measured in number of samples).

For fault identification, the fault compensated signals are filtered through the three baseline faulty models, reparametrized for the current operating conditions to generate three sets of sequences comprising of roll, pitch and yaw residuals. Binary hypothesis tests are designed on the properties of these residuals in order to determine the failed rotor.

Residual Variance Method The current 5-second-long signals ($N = 50$ samples sampled at 10 Hz frequency), with a time window update of 0.1 s, are driven through the VAR(2) model obtained from forward velocity and gross weight substitution into the VFP-VAR$(2)_9$ model for healthy aircraft to generate three sets of residual sequences. Fault detection is achieved through three parallel statistical hypotheses testing of the variance of the current residuals and the variance of the baseline residuals (Eq. 22). The baseline residuals for the current operating condition were estimated from "modelled" roll, pitch, and yaw residuals fitted with bivariate polynomials. The critical limit is determined from the F distribution's $(1-\alpha)$ critical limit for $(50,44)$ degrees of freedom (the total number of estimated parameters for the 3-variate VAR(2) model is 18). The statistical hypothesis test is conducted at the α (false alarm) risk level of 10^{-1} to minimize the false alarms. Indicative fault detection results for different states of the aircraft with gross weight 2.75 kg and flying at 6.5 m/s are presented in Fig. 11a.

To collect a minimum of 50 samples for testing, the test starts from 5 s. For current signals obtained from the healthy flight, the test statistics for each attitude signal fall below the critical limit denoting acceptance of the null hypothesis. A fault is detected whenever any of the test statistics violate the critical limit. With front and side rotor failure at 10 s, fault detection, which is evident from all three test statistics exceeding the critical limit, is immediate.

Post fault-compensation, signals of length 20 s ($N = 200$ samples), updated every 1 s have been filtered through the VAR models (for rotor failure, M_1, M_2 and M_6), reparametrized for current operating conditions to find the residual variances, σ^2_{1u}, σ^2_{2u} and σ^2_{6u} respectively (for roll,pitch and yaw residuals). These are compared statistically to the baseline residual variances σ^2_{11}, σ^2_{22} and σ^2_{66}, obtained from three bivariate polynomial models fitted to the roll, pitch, and yaw residuals obtained at specific operating conditions while identifying the three rotor failure VFP-VAR model models in the baseline phase. The statistical hypothesis test is designed at the α (false alarm) risk level of 10^{-2} to minimize the confusion between the various rotor failures.

Indicative results for a single time window at 5.5 m/s and 3.5 kg are presented in Figs. 12a to 12c. When all the test statistics for the roll, pitch, and yaw residual sequences obtained from model M_1 are within the critical limit, the fault is correctly classified as rotor 1 failure, as indicated in Fig. 12a. If any of the three statistics exceeds the critical limit, it is implied that the current faulty state is not related to rotor failure 1. Similarly, correct rotor failure identification has been made with residuals obtained from models M_2 and M_6, evident in Figs. 12b and 12c, respectively. If the test statistics of the residuals obtained from more than one model lie below the critical limit, it implies that there is confusion between those types of failure. Conversely, if all the test residuals from all the models exceed the critical limit, no decision is made on the type of rotor failure. As evident from the design of the test, multiple decisions or no decisions are possible for a single window of the signals. It can be observed that vector models perform better than scalar counterparts in failure classification, because they account for the cross-correlation between the multivariate signals.

Residual Uncorrelatedness Method Online fault detection by residual uncorrelatedness based on the identified vector model for current operating condition is performed

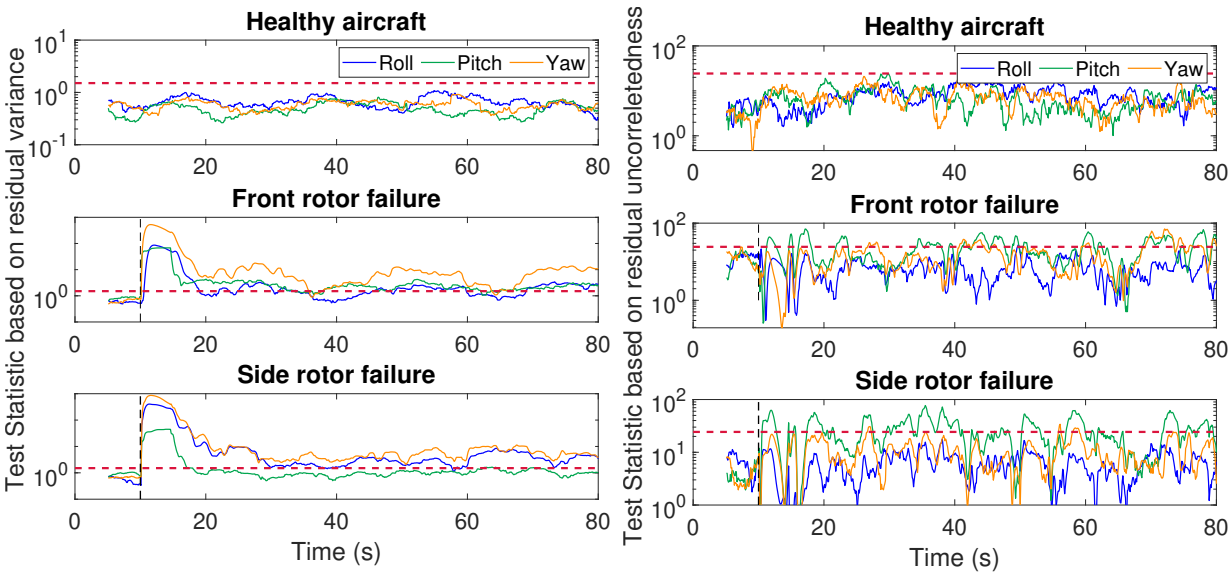

(a) Residual variance

(b) Residual uncorrelatedness

Figure 11: Indicative fault detection results based on the roll, pitch and yaw residual signals obtained via VFP-VAR model of healthy aircraft. The dashed vertical line represents the time of rotor failure. The dashed red horizontal line indicates the statistical threshold at the respective α risk levels. A fault is detected when nay of the statistics exceeds the threshold. (a) Residual variance method; operating condition: 6.5 m/s, 2.75 kg and $\alpha = 10^{-1}$ (b) Residual uncorrelatedness method; operating condition: 8.5 m/s, 2.25 kg and $\alpha = 10^{-3}$.

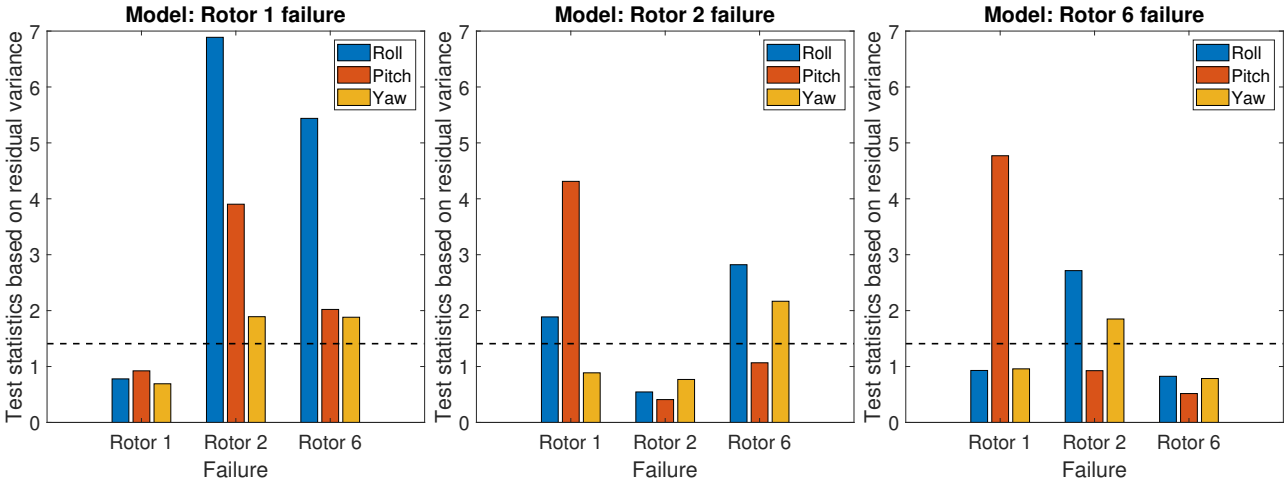

(a) Front rotor (1) failure

(b) Side rotor (2) failure

(c) Side rotor (6) failure

Figure 12: Indicative fault identification results by residual variance method based on the roll, pitch and yaw residual signals obtained via VFP-VAR model of different rotor failures at operating condition of 5.5 m/s and 3.5 kg. The dashed black horizontal line indicates the statistical threshold at the respective $\alpha = 10^{-2}$ risk level.

with 5 s ($N = 50$ samples) window length and update interval of 0.1 s for each residual sequence. In this method, the characteristic quantity is the autocorrelation function of the residuals with a maximum lag $\tau = 8$. The critical limit of the statistical hypothesis test is obtained as the $(1-\alpha)$ critical point of a χ^2 distribution with 8 degrees of freedom. Figure 11b shows three parallel hypothesis tests on roll, pitch, and yaw residuals obtained from 2.25 kg aircraft flying at 8.5 m/s and severe turbulence for different states of the aircraft: healthy aircraft, front, and side rotor failure, respectively, at the $\alpha = 10^{-3}$ risk level.

In the healthy case, the test statistic for all the three sig-

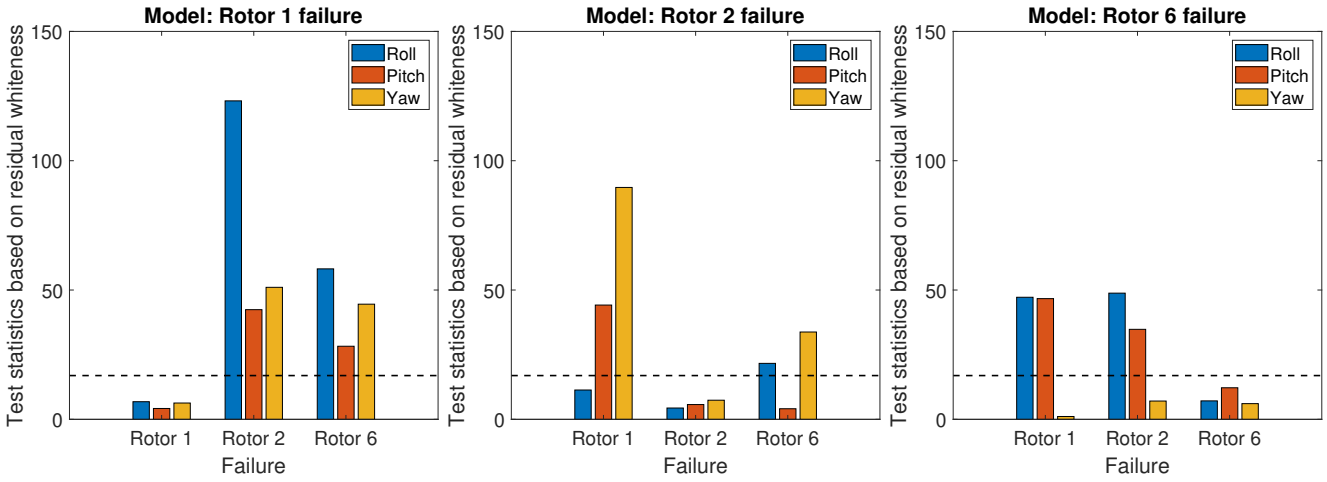

(a) Front rotor (1) failure (b) Side rotor (2) failure (c) Side rotor (6) failure

Figure 13: Indicative fault identification results by residual uncorrelatedness method based on the roll, pitch and yaw residual signals obtained via VFP-VAR model of different rotor failures at operating condition of 4.5 m/s and 3.25 kg. The dashed black horizontal line indicates the statistical threshold at the respective $\alpha = 0.05$ risk level.

nals is lower than the the critical limit, correctly declaring the system as healthy. For the front, and side rotor failure at 10 s, fault detection is fairly fast with any one of the test statistics exceeding the critical limit.

After the fault is compensated for by the controller, signals of length 20 s ($N = 200$ samples), updated every 1 s have been filtered through faulty models M_1, M_2 and M_6 to generate residual sequences $e_{1u}[t]$, $e_{2u}[t]$ and $e_{6u}[t]$, respectively, each containing roll, pitch, and yaw residuals. The autocorrelation function of each component of the residual sequences with maximum lag $\tau = 10$ has been considered as the test statistic to classify faults. Since the computation time required to classify failure is more than 0.3 s, the window update interval is kept at 1 s.

The results obtained from a single window of 20 s are shown in Figs. 13a through 13c. Figure 13a shows the residuals $e_{1u}[t]$ are uncorrelated (below $(1-\alpha)$ critical limit of a χ^2 distribution with 10 degrees of freedom). This signifies that the model (M_1) represents the dynamics of current state correctly and the fault is classified as failure of rotor 1. The models which do not represent the current aircraft state dynamics have correlated residuals (exceed the critical limit). Similarly, Figs. 13b and 13c show correct identification of the failure for rotors 2 and 6, respectively. This method can correctly identify rotor failures with vector models, in contrast to the scalar model approach.

CONCLUSIONS

A unified stochastic framework for rotor failure detection and identification in multicopters based on aircraft attitude signals has been developed. The method, capable of FDI under different operating conditions, turbulence, and uncertainty, has been based on the novel extended class of vector-dependent functionally pooled (VFP) models and proper statistical decision making schemes. "Global" statistical time series models, in the form of Vector Functionally Pooled AutoRegressive models (scalar and vector), can represent the hexacopter dynamics under various operating conditions in the presence of turbulence and uncertainty. These models, identified for healthy and different rotor failure scenarios, form the cornerstone of this residual based FDI technique. The theory for residual properties (variance and uncorrelatedness) based statistical hypothesis tests is discussed. Online rotor failure detection followed by identification with these methods coupled with the univariate and multivariate models has been demonstrated for a few test cases. The important conclusions from the study are summarized below:

- This study, with the proof-of-concept application, demonstrates effective fault detection and identification in multicopters flying under any condition within the operating range, turbulence, and uncertainty.
- The "global" statistical time series models based on aircraft response (*scalar* or *vector*) signals only, obtained under (i) ambient excitation due to turbulence and (ii) external white noise excitation, can fully

represent the important aircraft dynamics for different health status for the entire operating range.

- Simpler non–parametric approaches like the Power Spectral Density provide evidence of changing aircraft dynamics with different operating conditions. As the primary step of inspecting the collected signals, it justifies the need the for more complex functionally pooled models. It also provides validation of the final model parameters' dependencies on the forward velocity and gross weight.

- Both scalar and vector statistical time series methods have shown remarkable results in immediately detecting faults, with the vector methods achieving improved performance in case of fault classification with post-failure stationary signals.

- An impressive feat of these methods is that they are capable of distinguishing the faulty state from healthy aircraft even when the aircraft attitude signals have been compensated for and returned to a steady state by the controller after failure. Note that only the aircraft response signals have been utilized in this study without any knowledge of controller effort. Hence, parsimony of information while maintaining effectiveness of FDI has been achieved.

- Residual based rotor FDI under "unmodelled" or intermediate operating conditions, that is conditions not belonging to any of the considered operating conditions in training data (and thus not modelled in the baseline phase) has been successfully performed. Moreover, the baseline residual properties, on which these methods mainly rely on, have been estimated for "unmodelled" operating conditions, without corresponding baseline data. This has a substantial impact on the amount of training data needed to be generated in baseline phase.

- Another important achievement is that rotor FDI is possible without the need for active external excitation during the flight. This is established on the basis of the fact that the test data has been generated with only ambient excitation due to turbulence, in contrast to the training data having an active excitation too.

- In future, the rotor failure models will be appended with functional dependence on amount of rotor degradation, in order to be able to quantify the faults along with detection and classification. Also, sparse grid of training data with respect to different operating conditions coupled with orthogonal splines as basis functions will be explored. This will ease the limitation of uniformly spaced signals used in training the models.

AUTHOR CONTACT

Airin Dutta	duttaa5@rpi.edu
Michael McKay	mckaym2@rpi.edu
Fotis Kopsaftopolous	kopsaf@rpi.edu
Farhan Gandhi	fgandhi@rpi.edu

REFERENCES

1. "Urban Air Mobility (UAM) Market Study," Technical report, November 2018.

2. McKay, M., Niemiec, R., and Gandhi, F., "Post-Rotor-Failure-Performance of a Feedback Controller for a Hexacopter," American Helicopter Society 74th Annual Forum, Phoenix, AZ, May 2018.

3. Stepanyan, V., Krishnakumar, K., and Bencomo, A., "Identification and Reconfigurable Control of Impaired Multi-Rotor Drones," AIAA Science and Technology Forum and Exposition, January 2016.

4. Frangenberg, M., Stephan, J., and Fichter, W., "Fast Actuator Fault Detection and Reconfiguration for Multicopters," AIAA Guidance, Navigation, and Control Conference, January 2015. DOI: 10.2514/6.2015-1766

5. Heredia, G., and Ollera, A., "Sensor Fault Detection in Small Autonomous Helicopters using Observer/Kalman Filter Identification," IEEE International Conference on Mechatronics, Malaga, Spain, April 2009.

6. Qi, X., Theillol, D., Qi, J., Zhang, Y., and Han, J., "A Literature Review on Fault Diagnosis Methods for Manned and Unmanned Helicopters," International Conference on Unmanned Aircraft Systems, May 2013.

7. Fassois, S., and Kopsaftopoulos, F., "Statistical Time Series Methods for Vibration Based Structural Health Monitoring," *New Trends in Structural Health Monitoring*, edited by W. Ostachowicz and J. Guemes, Springer, January 2013, pp. 209–264. DOI: 10.1007/978-3-7091-1390-5

8. Kopsaftopoulos, F. P., and Fassois, S. D., "Scalar and Vector Time Series Methods for Vibration Based Damage Diagnosis in a Scale Aircraft Skeleton Structure," *Journal of Theoretical and Applied Mechanics*, Vol. 49, (4), 2011, pp. 727–756.

9. Samara, P. A., Fouskitakis, G. N., Sakellariou, J. S., and Fassois, S. D., "A Statistical Method for the Detection of Sensor Abrupt Faults in Aircraft Control Systems," *IEEE Transactions on Control Systems Technology*, Vol. 16, (4), July 2008, pp. 789–798. DOI: 10.1109/TCST.2007.903109

10. Kopsaftopoulos, F. P., and Fassois, S. D., "A vibration model residual-based sequential probability ratio test framework for structural health monitoring," *Structural Health Monitoring*, Vol. 14, (4), 2015, pp. 359–381.

11. Dimogianopoulos, D. G., Hios, J. D., and Fassois, S. D., "FDI for Aircraft Systems Using Stochastic Pooled-NARMAX Representations: Design and Assessment," *IEEE Transactions on Control Systems Technology*, Vol. 17, (6), November 2009, pp. 1385–1397.

12. Dimogianopoulos, D. G., Hios, J. D., and Fassois, S. D., "Aircraft Fault Detection and Identification by Stochastic Functionally Pooled Modelling of Relationships among Attitude Data," Proceedings of the Institution of Mechanical Engineers, Part G: Journal of Aerospace Engineering, Vol. 222, June 2008. DOI: 10.1243/09544100JAERO315.

13. Kopsaftopoulos, F. P., and Fassois, S. D., "Vector-dependent Functionally Pooled ARX Models for the Identification of Systems Under Multiple Operating Conditions," IFAC Proceedings, Vol. 45, 2012. DOI: 10.3182/20120711-3-BE-2027.00261.

14. Kopsaftopoulos, F. P., and Fassois, S. D., "A functional model based statistical time series method forvibration based damage detection, localization, andmagnitude estimation," *Mechanical Systems and Signal Processing*, Vol. 39, 2013, pp. 143–161.

15. Kopsaftopoulos, F., Nardari, R., Li, Y.-H., and Chang, F.-K., "A stochastic global identification framework for aerospace structures operating under varying flight states," *Mechanical Systems and Signal Processing*, Vol. 98, 2018, pp. 425–447.

16. Sakellariou, J. S., and Fassois, S. D., "Functionally Pooled Models for the Global Identification of Stochastic Systems under Different Pseudo-Static Operating Conditions," *Mechanical Systems and Signal Processing*, Vol. 72-73, May 2016, pp. 785–807. DOI: 10.1016/j.ymssp.2015.10.018

17. Hios, J., and Fassois, S., "A Global Statistical Model Based Approach for Vibration Response-only Damage Detection under Various Temperatures: A Proof-of-concept Study," *Mechanical Systems and Signal Processing*, Vol. 49, 2014, pp. 77–94. DOI: 10.1016/j.ymssp.2014.02.005

18. Dutta, A., McKay, M., Kopsaftopoulos, F., and Gandhi, F., "Rotor Fault Detection and Identification on a Hexacopter Based on Statistical Time Series Methods," Vertical Flight Society 75th Annual Forum, Philadelphia, PA, May 2019.

19. Dutta, A., McKay, M., Kopsaftopoulos, F., and Gandhi, F., "Fault Detection and Identification for Multirotor Aircraft by Data-Driven and Statistical Learning Methods," Electric Aircraft Technologies Symposium (EATS), Indianapolis, IN, August 2019.

20. Dutta, A., McKay, M., Kopsaftopoulos, F., and Gandhi, F., "Statistical Time Series Methods for Multicopter Fault Detection and Identification," Vertical Flight Society International Powered Lift Conference, San Jose, CA, Jan 2020.

21. Peters, D., and He, C., "A Finite-State Induced Flow Model for Rotors in Hover and Forward Flight," American Helicopter Society 43rd Annual Forum, St. Louis, MO, May 1987.

22. Hakim, T. M. I., and Arifianto, O., "Implementation of Dryden Continuous Turbulence Model into Simulink for LSA-02 Flight Test Simulation," Journal of Physics: Conference Series 1005(2018) 012017, August 2018.

23. Tischler, M. B., and Remple, R. K., *Aircraft and Rotorcraft System Identification*, AIAA, second edition, 2012.

24. Niemiec, R., and Gandhi, F., "Multi-Rotor Coordinate Transforms for Orthogonal Primary and Redundant Control Modes for Regular Hexacopters and Octocopters," 42nd Annual European Rotorcraft Forum, Lille, France, September 2016.

25. Greene, W. H., *Econometric Analysis*, Prentice Hall, fifth edition, 2003.

26. Kopsaftopoulos, F. P., and Fassois, S. D., "Vector-dependent Functionally Pooled ARX Models for the Identification of Systems Under Multiple Operating Conditions," 16th IFAC Symposium on System Identification The International Federation of Automatic Control, Brussels, Belgium, Vol. 46, 2012.

27. Ljung, L., *System Identification: Theory for the User*, Prentice–Hall, second edition, 1999.

28. Söderström, T., and Stoica, P., *System Identification*, Prentice–Hall, 1989.

29. Lütkepohl, H., *New Introduction to Multiple Time Series Analysis*, Springer-Verlag Berlin, 2005.

30. Dunkl, C., and Xu, Y., *Orthogonal Polynomials in Several Variables*, Cambridge University Press, 2001.

31. Krall, H., and Scheffer, I., "Orthogonal polynomials in two variables," *Annali di Matematica Puraed Applicata*, Vol. 76, 1967, pp. 325–376.

32. Kowalski, M., "The recursion formulas for orthogonal polynomials innvariables," *SIAM Journalon Mathematical Analysis*, Vol. 13, 1982, pp. 309–315.

APPENDIX

A. Bivariate Polynomials

Bivariate (two-dimensional) orthogonal polynomials may be obtained as tensor products from their corresponding (Chebyshev, Legendre, Jacobi, or other (Refs. 30–32)) univariate counterparts. For example, the bivariate Chebyshev orthogonal polynomials have the following form:

$$\begin{aligned} P_{mn}(x,y) &= P_m(x)\cdot P_n(y) \\ (x,y) &\in [-1,1]\times[-1,1]\subset\mathbb{R}^2 \end{aligned} \tag{29}$$

with P_{mn} the bivariate Chebyshev polynomial of total degree mn and $P_m(x), P_n(y)$ the univariate Chebyshev polynomials of degrees m, n, respectively.

Construction of bivariate polynomial orthogonal basis (Refs. 31, 32)

A polynomial orthogonal basis of maximum degree mn contains a total of $\frac{1}{2}(mn+1)(mn+2)$ basis functions obtained as follows:

1. Constant basis function	$P_{0,0}$
2. Linear basis functions	$P_{1,0}, P_{0,1}$
3. Quadratic basis functions	$P_{2,0}, P_{1,1}, P_{0,2}$
4. Cubic basis functions	$P_{3,0}, P_{2,1}, P_{1,2}, P_{0,3}$
⋮	
$mn+1$. degree mn basis functions	$P_{mn,0}, P_{mn-1,1}, \ldots, P_{1,mn-1}, P_{0,mn}$

The univariate polynomials used in this study in order to obtain their bivariate counterparts are the shifted Chebyshev polynomials of the second kind (Type II Chebyshev polynomials), which belong to the broader family of Chebyshev orthogonal polynomials. These polynomials obey the following recurrence relation:

$$\begin{aligned} a_{1,n}G_{n+1}(x) &= (a_{2,n}+a_{3,n}x)G_n(x) - a_{4,n}G_{n-1}(x) \\ x &\in [0,1]\subset\mathbb{R} \end{aligned} \tag{30}$$

with $a_{1,n} = a_{4,n} = 1, a_{2,n} = -2, a_{3,n} = 4$, and $G_0(x) = 0, G_1(x) = 1$.

Hence, the first five shifted Chebyshev polynomials of the second kind are:

$$\begin{aligned} P_0 &= 1 \\ P_1 &= -1+2x \\ P_2 &= 1-8x+8x^2 \\ P_3 &= -1+18x-48x^2+32x^3 \\ P_4 &= 1-32x+160x^2-256x^3+128x^4 \end{aligned} \tag{31}$$

In the present framework, where the two variables are forward velocity (k^1) and gross weight (k^2), the following variable selections are made:

$$\begin{aligned} x &\in [0,1]\subset\mathbb{R}, \quad x = k^1/k^1_{max} \\ y &\in [0,1]\subset\mathbb{R}, \quad y = k^2/k^2_{max} \end{aligned} \tag{32}$$

B. Model Validation

The Q-statistics is given by $Q = N(N+2)\cdot\sum_{\tau=1}^{r}(N-\tau)^{-1}\cdot\widehat{\rho}[\tau]^2 \sim \chi^2(r)$, where $\widehat{\rho}[\tau]$ designates the residual series normalized autocorrelation at lag, τ and it follows a $\chi^2(r)$ distribution with 'r' degrees of freedom. In Figs. 14a and 14b the red dashed line is 99% confidence limit ($\alpha = 0.01$) for $\chi^2(50)$ distribution. If the Q-statistics lie below the $(1-\alpha)$ critical limit of the distribution, the residuals are considered to be white or uncorrelatedness. The models are validated based on the fact that the models correctly representing the system dynamics should generate a white (uncorrelated) residual sequences for all cross-sections. In Figs. 14a and 14b the Q-statistics of all the cross-sections have been presented in grids, with the forward velocity shown in the top and gross weight shown in the right. Since, vector models generate three residuals, namely roll, pitch, and yaw residuals, the grids in Fig. 14b have three bars representing the Q-statistics.

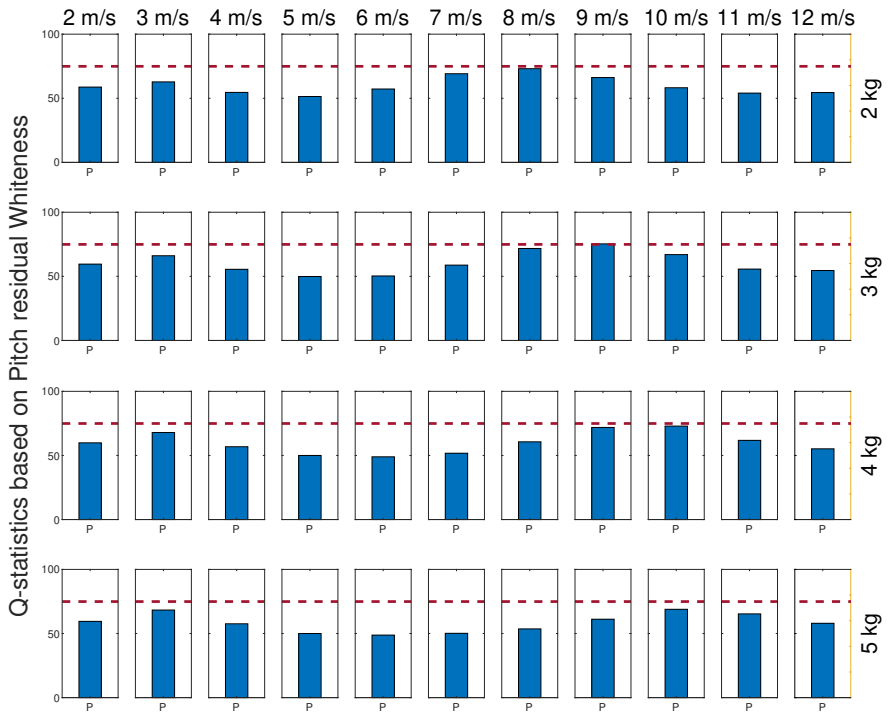

(a) VFP-AR model

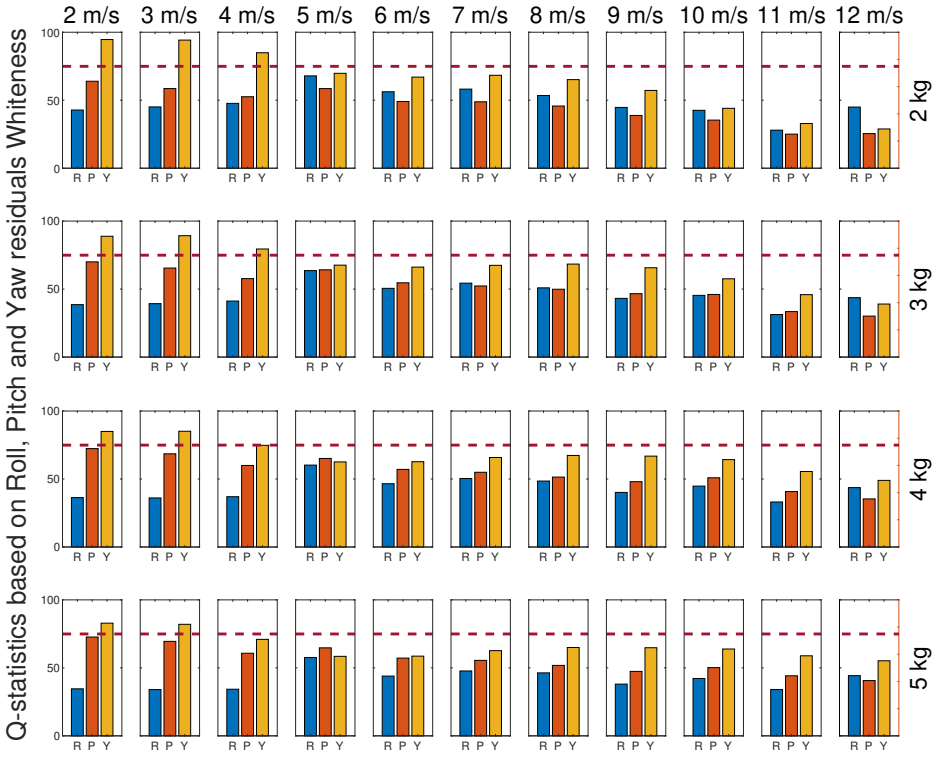

(b) VFP-VAR model

Figure 14: VFP Model validation of healthy by examination of residual uncorrelatedness for all-cross sections (a) AR model estimated with Pitch signals only and (b) VAR model estimated with Roll, Pitch and Yaw signals. The red horizontal dashed line is the 99% confidence limit.

C. Power Spectral Density

The Figs. 15a and 15b, shows the indicative PSD magnitude curves obtained from VFP-AR$(15)_9$ model of a healthy aircraft based on pitch signals. It can be observed that the dynamics of the healthy aircraft changes with the forward velocity but is constant with the gross weight.

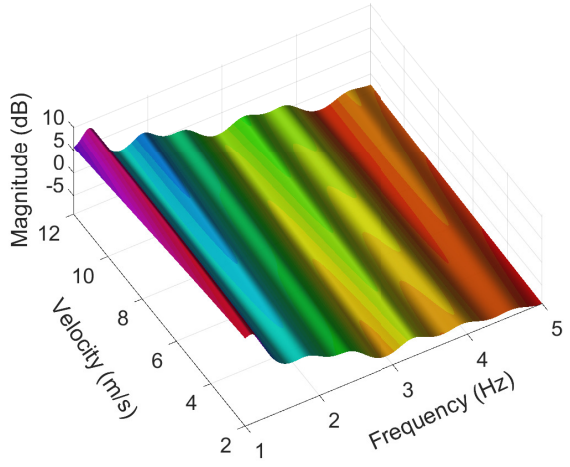

(a) Frequency change with forward velocity

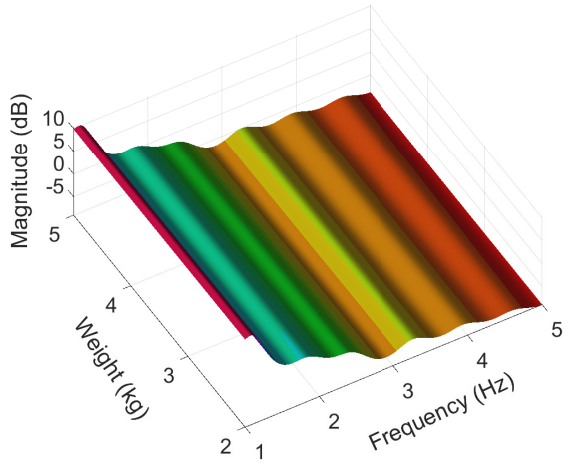

(b) Frequency change with gross weight

Figure 15: VFP-AR$(15)_9$ based PSD magnitude versus frequency and (a) forward velocity and (b) gross weight